Machine Learning guided exploration of ternary metal borohydrides

Rong Cheng,[1,2] Xuyan Xue[1] and C. Z. Wang[2]*

[1]*College of Physics, Qingdao University, Qingdao, Shandong 266071, China*
[2]*Ames Laboratory-U.S. DOE and Department of Physics and Astronomy, Iowa State University, Ames, IA 50011, U.S.A*

Abstract

We employ deep machine learning (ML) combined with first-principles calculations to explore energetically favorable ternary metal borohydrides. Using La-B-H as a prototype system, we demonstrate that iteratively trained ML models can efficiently screen hundreds of thousands of hypothetical structures and accurately select a small fraction of promising structures and compositions for further studies by first-principles calculations. Such an ML-guided approach dramatically accelerates the pace of materials discovery. A number of new La-B-H ternary compounds with formation energies within 100 meV/atom above the known ternary convex hull are discovered, including a known stable $La(BH_4)_3$ phase. Moreover, by replacing La with Group 1, 2, 3, 13, and 14 elements in the four lowest-energy La-B-H structures from our ML-guided predictions, several low-energy X-B-H (X=Mg, Ca, Sr, Ba, Sc, Y, Ac, Al, Ga, In, Si, Ge, Sn, Pb) compounds are predicted.

1. Introduction

Complex metal borohydrides have attracted considerable interests over the past decades as potential materials for hydrogen or thermal energy storage [1-5], solid state electrolytes [6,7], catalysis [8,9], luminescence [10,11]. It has also been shown that metal borohydrides can be unique magnetic functional materials [12,13] as well as promising ambient-pressure high-temperature superconductors [14–18].

At first, borohydrides of alkali and alkaline earth metals, such as $LiBH_4$ and $Mg(BH_4)_2$, were intensively studied due to their high gravimetric hydrogen storage capacity. However, their decomposition temperatures are too high and rehydrogenation only occurs under severe conditions [3]. Borohydrides containing trivalent or transition metal cations such as $Al(BH_4)_3$ and $Y(BH_4)_3$ can retain high gravimetric hydrogen density, but they are thermodynamically unstable with decomposition temperatures slightly above room temperature [19]. In contrast, rare earth (RE) metal borohydrides are able to release a major amount of hydrogen between 200 and 300 ^{o}C. Unfortunately, they possess lower gravimetric hydrogen density [20].

The corresponding author's E-mail: wangcz@ameslab.gov

On the other hand, alkali metal *closo*-dodecaborates $A_2B_{12}H_{12}$ (A = Li, Na, K) and alkaline earth metal *closo*-dodecaborates $AeB_{12}H_{12}$ (Ae= Mg, Ca) were first known as intermediate compounds in the decomposition process of the related borohydrides (ABH_4 and $Ae(BH_4)_2$) [21–23]. The discovery of high ionic conductivity in alkali metal dodeca- or deca- borohydrides [24,25] renewed interest in these materials as potential solid state electrolytes [6,26,27]. As for alkaline earth metal *closo*-dodecaborates, such $CaB_{12}H_{12}$ and $MgB_{12}H_{12}$, the low cationic diffusivity may hinder their practical use even though they possess reasonably good electrochemical stability [7].

Recently, metal borohydrides have been demonstrated to be a promising playground to hunt for high-T_c superconductors near ambient pressure. For instance, KB_2H_8 was found to become a superconductor with T_c about 140 K at 12 GPa [14,15]. Doping holes into α-$Ca(BH_4)_2$ was suggested to exhibit room-pressure superconductivity above 110K [16]. Also, doping holes into $Mg(BH_4)_2$ was also predicted to exhibit room-pressure superconductivity up to ~ 140K very recently [17]. Moreover, it has been shown by first-principles density functional theory (DFT) calculations that by charge transfer modulating via the replacement of Ca with alkali metal atoms, e.g., Cs, the structure of $CaBH_5$ predicted above 280GPa can maintain its dynamical stability with pressure down to 1GPa, and $CsBH_5$ is a superconductor with transition temperature as high as 98 K [18].

Despite extensive studies, the composition-structure-property space of metal borohydrides is still largely unexplored due to the vast numbers of possibilities in the combinations of compositions and crystal structures for 3 or more chemical elements in metal borohydrides. In particular, no comprehensive studies of the structures and properties of transition or RE metal *closo*-borates and their families have been reported. Therefore, accelerating the exploration of novel B-H anions and borohydrides for applications as hydrogen storage materials, solid state electrolytes and superconductors near ambient pressure are highly desired.

In this paper, we explore novel energetically favorable ternary compounds of metal borohydride using deep machine learning (ML) guided first-principles calculations. The efficiency of this approach, especially iteratively trained ML models in accelerated selecting promising structures and compositions for further first-principles calculations, is demonstrated. We discovered a number of low-energy La-B-H ternary compounds with formation energies less than 100 meV/atom relative to that of the convex hull. In particular, two $La(BH_4)_3$ and two $La(BH)_{12}$ phases are predicted to be stable or within 10 meV/atom above the convex hull. Moreover, by replacing La with Group 1, 2, 3, 13, and 14 elements in the four lowest-energy La-B-H structures, we predict a series of low-energy ternary metal borohydrides.

The rest of the article is organized as follows. In section 2, we describe in detail how low-energy Lanthanum borohydride compounds are efficiently predicted by an ML-guided framework.

Exploration of more metal borohydride compounds by substituting La with other metal elements is reported in section 3. Finally, a summary is given in section 4.

2. Methods

We take Lanthanum borohydrides as a prototype to predict new ternary metal borohydrides using an ML-guided framework. Even though the three chemical elements (La, B, and H) are given, the search for energetically favorable ternary compounds is still very challenging because the number of possible combinations of composition ratio among the three elements and the potential crystal structure they may take is enormous. It is impossible to search for low-energy structures for all these combinations using the state-of-the-art crystal structure prediction methods such as genetic algorithm (GA) or particle swarm optimization (PSO) [28–30]. Straightforward calculations by first-principles methods [31–33] are computationally very expensive and time-consuming.

We employ a crystal graph convolutional neural network (CGCNN) ML model [34] to guide the efficient high-throughput screening and the selection of promising candidates for further optimization by first-principles DFT calculations. Such an approach has been shown to be efficient in accelerating the discovery of novel materials and has been demonstrated in searching for ternary compounds [35,36], magnetic materials [37], and superconductors at ambient pressure [38], where some theoretical predictions have been successfully confirmed by experiments [35–37].

In CGCNN [34], a crystal structure is represented by a crystal graph, which encodes both atomic information and bonding interactions between atoms. A convolutional neural network is then built on top of the graph to construct the proper descriptors that are optimal for predicting the target properties. First, we train the first generation CGCNN model (1G-CGCNN) for predicting the formation energy E_f of compounds, using the DFT calculated structures and energies of 59,028 ternary compounds (including one known La-B-H compound $La(BH_4)_3$) from the Materials Project (MP) database. Here the formation energy E_f is defined relative to the energies of the elemental bulk phases of the three constituent elements. For any ternary structure $X_mY_nZ_k$, E_f is defined as:

$$E_f = \frac{E(X_mY_nZ_k) - mE(X) - nE(Y) - kE(Z)}{m+n+k}, \quad (1)$$

where $E(X_mY_nZ_k)$ is the total energy of the $X_mY_nZ_k$ compound. $E(X)$, $E(Y)$ and $E(Z)$ are the energy (per atom) of the ground state crystal structures with pure X, Y, and Z element, respectively.

The database was randomly divided into a training set (80%), validation set (10%) and test set (10%). Parameters are mostly set to default values under the guidance of Ref. [34]. Batch size is set to 256 and total number of epochs to run is set to 300. The best-performing model that provides the lowest mean absolute error (MAE) for the validation set is selected from all 300 epochs during the computation. The comparison between the 1G-CGCNN predicted values and the DFT calculated

values of MP is shown in Figure 1a. It can be seen that the 1G-CGCNN model describes well the formation energies of these ternary compounds, with the MAE only 0.063 eV/atom.

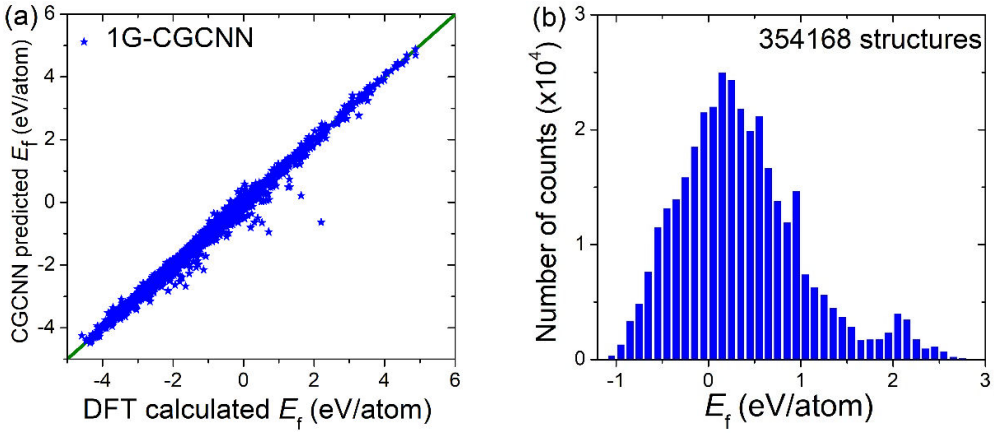

Figure 1. (Color online) (a) Formation energies E_f predicted by the 1G-CGCNN are compared with the results of DFT calculations from Materials Project. (b) Distribution of formation energies E_f for 354168 hypothetical La-B-H ternary compounds predicted by the 1G-CGCNN.

To search for new low-energy ternary La borohydrides over a wide range of compositions, we replace the three elements on the lattices of the above 59,028 ternary structures from the MP database by La, B, and H. Since there are six ways to shuffle the three elements on a given template ternary structure, we generate 354,168 ternary La-B-H hypothetical structures. Then, we apply the 1G-CGCNN ML model to predict the formation energies E_f for these hypothetical ternary borohydrides. 112190 ternary compounds covering more than 4000 different La-B-H compositions are predicted to have negative formation energies. The formation energy distribution from the 1G-CGCNN prediction is shown in Figure 1b. We select the lowest energy structures with different symmetries in each chemical formula and obtain 16458 structures with $E_f < 0$. Then, we screen out 2429 with E_f less than -0.2 eV/atom and a composition ratio of La $\leq$ 0.5 for further optimization by first-principles DFT calculations.

The first-principles DFT calculations are carried out using the projector augmented wave method [39] as implemented in the VASP code [40]. The exchange and correlation energy functional are treated by the generalized gradient approximation (GGA) and parameterized by the Perdew-Burke-Ernzerhof formula (PBE) [41]. A plane-wave basis set with a kinetic energy cutoff of 400 eV was used to expand the electronic wave functions, and the convergence criterion for the total energy was set to 10^{-4} eV. The Monkhorst-Pack's sampling scheme [42] is adopted for Brillouin zone sampling with a k-point grid of $2\pi \times 0.04$ Å^{-1}, and the unit cell lattice vectors (both the unit cell shape and size) are fully relaxed together with the atomic coordinates until the force on each atom is < 0.01 eV × Å^{-1}.

Finally, we obtain 1249 converged structures from the DFT calculations based on the candidates selected from the 1G-CGCNN prediction. Among these structures, the known La-B-H ternary compounds $La(BH_4)_3$ with Pa-3 symmetry is found.

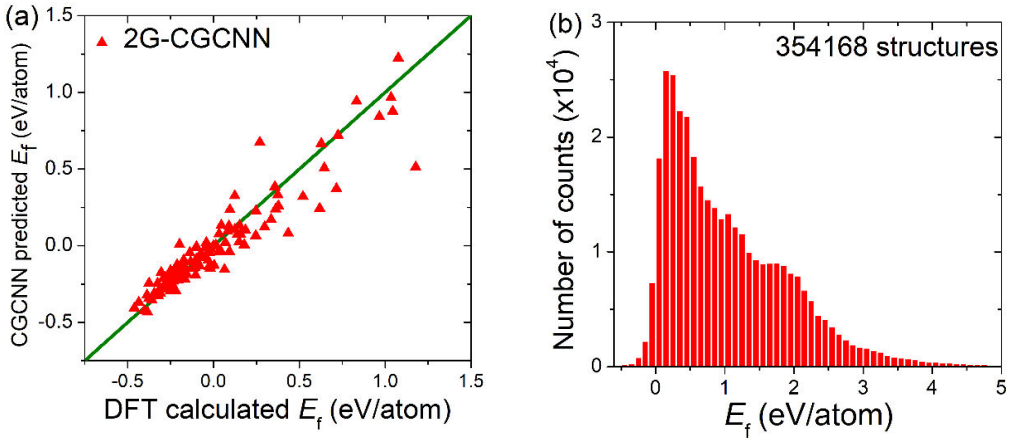

Figure 2. (Color online) (a) Formation energies E_f predicted by the 2G-CGCNN are compared with the results by DFT. (b) Distribution of formation energies E_f for 354168 hypothetical La-B-H ternary compounds predicted by the 2G-CGCNN.

Using structures and energies of the 1249 La-B-H ternary compounds obtained by DFT, we train the second-generation CGCNN model (2G-CGCNN) specifically for the La-B-H system. The training accuracy is shown in Figure 2a where the validation MAE is about 0.116 eV/atom. Then, we apply the 2G-CGCNN model to predict the formation energy E_f of the 354,168 ternary La-B-H hypothetical compounds. The formation energy distribution from the 2G-CGCNN prediction is shown in Figure 2b. After screening, a total of 2321 structures with $E_f < 0$ are selected. Compared these 2321 structures with the 2429 structures selected from the 1G-CGCNN model, we obtain 2224 different structures. Then, we relax these 2224 structures by first-principles DFT calculations and find 1328 converged structures.

To further investigate the energetic stability of the structures at different compositions, the formation energy E_d with respect to the known convex hull of the ternary system (namely, the energy distance from the known convex hull) is also calculated using the structures and energies of the 2577 compounds from the DFT calculations based on the selections from the 1G- and 2G-CGCNN models. E_d of any given phase on the ternary convex hull can be calculated by comparing its formation energy with respect to the nearby three known phases on the convex hull. These three known phases can be ternary, binary, or elementary crystalline phases, and the chemical compositions of these three phases are located at the vertexes of a triangle (called a Gibbs triangle) that encloses the composition of the phase for which E_d is calculated. Therefore, E_d determines the thermodynamic stability of the given phase against decomposition into the nearby three known phases. The calculated convex hull phase

diagram of the La-B-H system is shown in Figure 3.

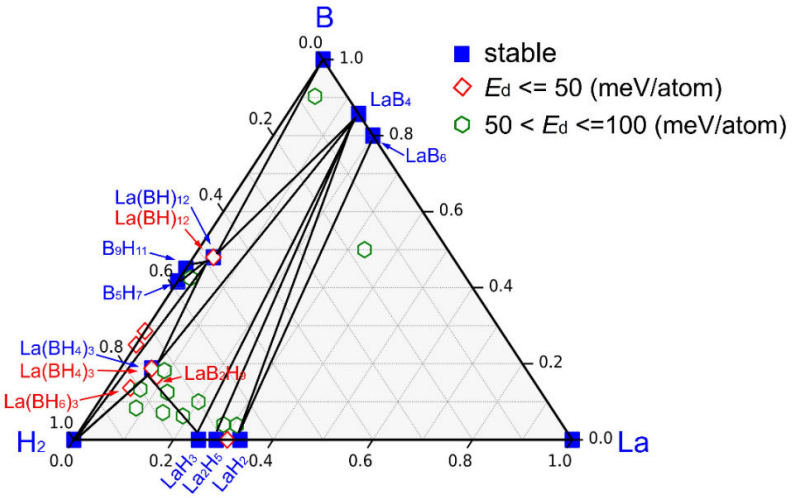

Figure 3. (Color online) Ternary phase diagram of the La-B-H system. All calculations are carried out at 0 K. Blue solid square represents stable phase, red hollow diamond indicates the metastable phase with E_d less than 50 meV/atom while green hollow hexagon indicates the metastable phase with E_d between 50 meV/atom and 100 meV/atom.

3. Results and Discussion

3.1. ML-Guided Predictions of Ternary Lanthanum Borohydride Compounds

The information on the predicted stable and metastable compounds with E_d < 100 meV/atom is given in Table 1. In addition to capturing one known ternary compound $La(BH_4)_3$ with Pa-3 symmetry, our ML-guided DFT calculations reveal another stable La-B-H ternary compound $La_2B_{24}H_{24}$ ($La(BH)_{12}$). We find two $La(BH)_{12}$ structural polymorphs, where one with P31c symmetry is stable while the other with C2/c symmetry is metastable with a formation energy only 8 meV/atom above the convex hull. Moreover, 28 more metastable La-B-H ternary compounds with the formation energy within 100 meV/atom above the convex hull are also predicted. A $La(BH_4)_3$ polymorph with Fm3-c symmetry with a formation energy only 12 meV/atom higher than the known Pa-3 symmetry. The structures of the two $La(BH_4)_3$ polymorphs and two $La(BH)_{12}$ polymorphs are plotted in Figure 4(a)-(d), respectively.

The known $La(BH_4)_3$ compounds, denoted as $La(BH_4)_3$-A in Figure 4(a), has Pa-3 symmetry and each La^{3+} cation interacts with six nearest neighboring $(BH_4)_3^-$ units via 12 La-H bonds, while each $(BH_4)_3^-$ anion is linked by two La^{3+} cations. Our predicted $La(BH_4)_3$ compound, denoted as $La(BH_4)_3$-B in Figure 4(b), has a higher symmetry space group, Fm3-c, and the La cation is coordinated to six $(BH_4)_3^-$ nearest neighbors with the same La-H bonds of 2.43 Å.

Table 1. Composition, Space Group, and Formation energy E_d of 31 La-B-H Compounds with E_d < 100 meV/atom at Ambient Pressure[a].

Composition	Space Group	E_d (meV/atom)	Generation
$La_8B_{24}H_{96}$ ($La(BH_4)_3$)	Pa-3	0	1G/2G
$La_2B_{24}H_{24}$ ($La(BH)_{12}$)	P31c	0	1G/2G
$La_2B_{24}H_{24}$ ($La(BH)_{12}$)	C2/c	8	1G/2G
$La_2B_4H_{18}$ (LaB_2H_9)	Cc	10	2G
$La_8B_{24}H_{96}$ ($La(BH_4)_3$)	Fm3-c	12	1G/2G
$La_2B_4H_{18}$ (LaB_2H_9)	P-1	38	2G
$La_2B_6H_{36}$ ($La(BH_6)_3$)	P-3	42	2G
$La_2B_2H_{12}$ ($LaBH_6$)	P2_1	61	2G
$La_2B_4H_{16}$ ($La(BH_4)_2$)	C2/c	62	1G/2G
$La_2B_4H_{16}$ ($La(BH_4)_2$)	Fddd	63	1G/2G
$La_2B_4H_{16}$ ($La(BH_4)_2$)	Fdd2	63	1G/2G
$La_2B_{40}H_{52}$ ($La(B_{10}H_{13})_2$)	C2/c	69	2G
$La_2B_4H_{16}$ ($La(BH_4)_2$)	I-42d	72	1G/2G
$La_3B_6H_{24}$ ($La(BH_4)_2$)	R3	74	1G
La_3BH_{12}	Pm	80	2G
$La_8B_{12}H_4$ (La_2B_3H)	P-6m2	82	2G
$La_8B_{12}H_4$ (La_2B_3H)	P-6	82	2G
$La_4B_4H_{40}$ ($LaBH_{10}$)	Ibca	84	2G
$La_2B_4H_{16}$ ($La(BH_4)_2$)	P-1	85	1G
La_7BH_{17}	P1	86	2G
La_8BH_{17}	C2/m	89	2G
$La_2B_4H_{16}$ ($La(BH_4)_2$)	Pmc2_1	90	1G/2G
$La_4B_2H_{22}$ (La_2BH_{11})	Pmc2_1	91	2G
$LaB_{28}H_2$	Cm	92	2G
La_3BH_{12}	Pm	92	2G
$La_6B_6H_{36}$ ($LaBH_6$)	C2/c	92	1G/2G
LaB_2H_{12} ($La(BH_6)_2$)	P-1	94	2G
$La_2B_4H_{16}$ ($La(BH_4)_2$)	P-4	94	1G/2G
$La_2B_4H_{16}$ ($La(BH_4)_2$)	P4_2/m	95	1G/2G
$La_2B_4H_{16}$ ($La(BH_4)_2$)	P4_2	97	1G/2G
La_2BH_7	P1	98	2G

[a]The fourth column represents the generation of CGCNN model where the structures is predicted.

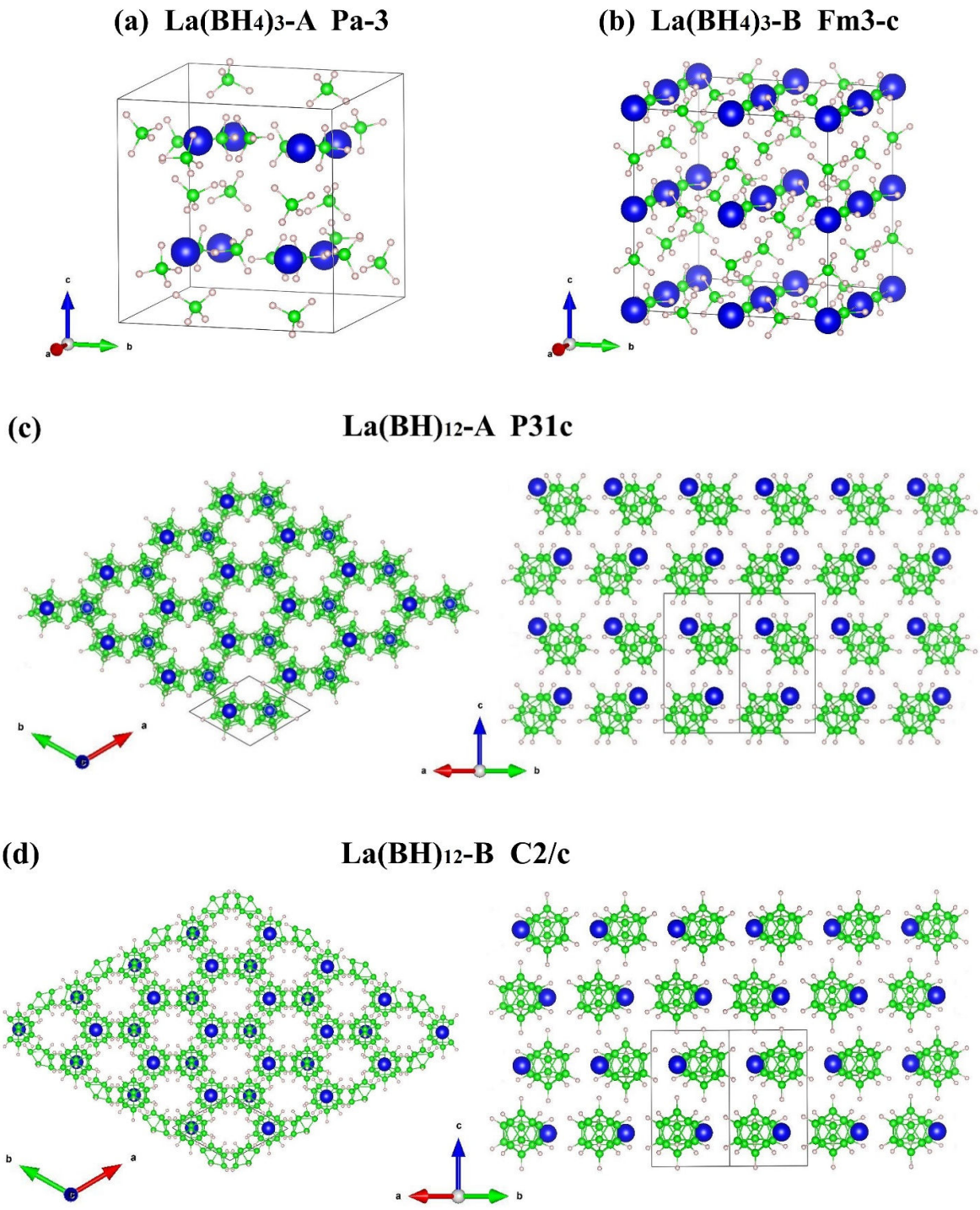

Figure 4. (Color online) Crystal structures of two lowest-energy $La(BH_4)_3$ polymorphs and two lowest-energy $La(BH)_{12}$ polymorphs obtained from our ML-DFT predictions. (a) and (b) Perspective views of $La(BH_4)_3$-A and $La(BH_4)_3$-B, respectively. (c) Top (left) and side (right) views of $La(BH)_{12}$-A and (d) top (left) and side (right) views of $La(BH)_{12}$-B. Blue (big) balls, green (medium), and pink (small) balls represent La, B, and H atoms, respectively.

In the predicted $La(BH)_{12}$ structure with P31c symmetry, denoted as $La(BH)_{12}$-A in Figure 4(c), each La^{2+} cation interacts with four nearest neighboring $(BH)_{12}^{2-}$ anions via 12 H atoms, while each $(BH)_{12}^{2-}$ anion is surrounded tetrahedrally by four cations. The structure is similar to the P31c structural arrangements for $Sr(BH)_{12}$ and $Ba(BH)_{12}$ [43], which represents the preferred arrangement of Ae^{2+} cations and $(BH)_{12}^{2-}$ anions for Ae^{2+} cations above certain size. Interestingly, another predicted $La(BH)_{12}$ structure with C2/c symmetry, denoted as $La(BH)_{12}$-B in Figure 4(d), is isostructural to $Ca(BH)_{12}$ known phase [44]. This type of structure displays cations surrounded by five neighboring $(BH)_{12}^{2-}$ anions. Three $(BH)_{12}^{2-}$ anions form the triangular equatorial plane centered on one La^{2+} cation, while the other two $(BH)_{12}^{2-}$ anions are in axial positions. As shown in the top view (left panel) of Figure 4(c) and 4(d), both $La(BH)_{12}$-A and $La(BH)_{12}$-B polymorphs have an extended network of metal cations linked by the close-*dodecaborate* $(BH)_{12}$ units to form periodic porous structures.

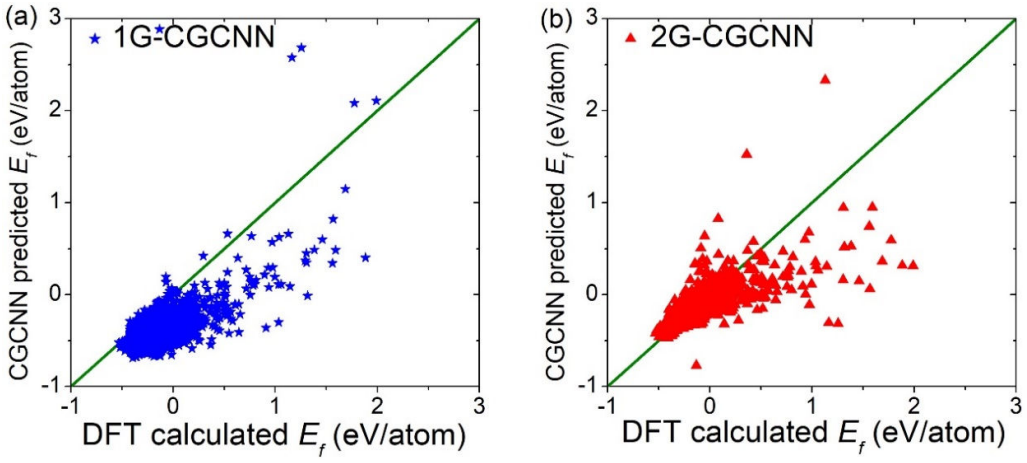

Figure 5. (Color online) Comparison between the 1G- (a) and 2G-CGCNN (b) predicted values and the DFT-calculated values of 1328 La-B-H structures.

By comparing the E_f distributions from the 1G-CGCNN and the 2G-CGCNN shown in Figure 1(b) and Figure 2(b) respectively, we can see that the 1G-CGCNN predicts much more La-B-H compounds having negative E_f than the predictions from the 2G-CGCNN. However, many stable and low-energy metastable compounds predicted from the 2G-CGCNN and confirmed by the DFT calculations as shown in Table 1 are missed by the 1G-CGCNN, while almost all the valid predictions from the 1G-CGCNN are recaptured by the 2G-CGCNN. This comparison suggests that the 2G-CGCNN trained using only the La-B-H data is much more accurate than the 1G-CGCNN, which is trained using the data covering almost all the elements in the periodic table. To verify this, we apply the 1G- and 2G-CGCNN models, respectively, to predict the formation energy E_f of the 1328 ternary

La-B-H compounds optimized by the DFT calculations based on the selection from the 2G-CGCNN. These DFT data are not included in the training of the 1G and 2G CGCNN models. The comparison of E_f from the GCGNN predictions and DFT calculation for this set of structures are shown in Figure 5. The MAE of the 1G-CGCNN prediction is 0.261 eV/atom, while the 2G-CGCNN model has a much lower MAE of 0.119 eV/atom. Also, the 1G-CGCNN model predicts E_f of La-B-H ternary compound systematically below the DFT calculated values. The comparison confirms that the 2G-CGCNN model is much more accurate than 1G-CGCNN. While the 1G-CGCNN model, which is more general since it is trained on data involving many chemical elements, can be used as an initial model for any compounds of interest, our study suggets that more accurate and reliable CGCNN models can be trained iteractively by including the relavent data for the specific systems from the previous CGCNN selction and DFT validation cycles.

3.2. Exploring More Metal Borohydride Ternary Compounds

For univalent (mainly alkali) and divalent (mainly alkaline earth metal), their *closo*-dodecaborates borohydrides have been studied extensively [24,26,43–45], but the structural and properties of metal borohydrides with tri- or tetravalent cations are relatively less known. It would be interesting to see what type of *closo*-dodecaborates borohydride structure is favored for different valent cations.

Based on the four lowest-energy structure motifs from our ML-guided search for La-B-H ternary compounds shown in Figure 4, we substitute La with groups 1, 2, 3, 13, and 14 elements to explore the stability of the ternary metal borohydride compounds. The formation energy relative to the convex hull of the substituted $X(BH)_{12}$-A and $X(BH)_{12}$-B (X = Sc, Y, Ac, Mg, Ca, Sr, Ba, Al, Ga, In, Tl, Si, Ge, Sn and Pb) compounds after first-principles DFT optimization is shown in Table 2. Corresponding substitution of $X(BH_4)_3$-A and $X(BH_4)_3$-B compounds are listed as well.

By substituting the La atoms of $X(BH)_{12}$-A and $X(BH)_{12}$-B compounds with groups 1, 2, 3, 13, and 14 elements, we note that the cation size does affect the structural characteristics of the metal *closo*-dodecaborates. As can be seen from Table 2, the most stable structure goes from $X(BH)_{12}$-B to $X(BH)_{12}$-A with the atomic size increasing in each group. The effects of cation size on the structural features of the metal *closo*-dodecaborates have been observed in the alkaline earth metal substituted $X(BH)_{12}$ (X = Mg, Ca, Sr, Ba) compounds [43]. Generally speaking, the variation in the structural arrangements follows simple geometric packing criteria. 2-fold coordination is favored for ratios below 0.155. Planar 3-fold coordination is favored when the cation–anion radius ratio r_c/r_a is between 0.155 and 0.225. Tetrahedral 4-fold coordination is favored for larger ratios between 0.225 and 0.414. Our results complete the known set of structures for $X(BH)_{12}$ compounds and provide a better understanding of their structural trend, in terms of the size of the cation. Our results also reveal a number of new stable or good metastable metal *closo*-dodecaborates compounds.

Table 2. Comparison of the Formation Energy above the Convex Hull for the Four lowest-energy La-B-H Structures with La Being Substituted by the Groups 1, 2, 3, 13, and 14 Elements[a]

X =	$X(BH_4)_3$-A (Pa-3)	$X(BH_4)_3$-B (Fm3-c)	$X(BH)_{12}$-A (P31c)	$X(BH)_{12}$-B (C2/c)
La	**0**	**12**	**0**	**8**
Sc	**0**	**1**	**25**	**0**
Y	**0**	**0**	**16**	**0**
Ac	**0**	**17**	**0**	**1**
Mg	211	225	**25**	**0**
Ca	196	211	**0**	**0**
Sr	131	154	**1**	**6**
Ba	215	243	**5**	**15**
Al	**6**	**91**	**13**	**0**
Ga	**53**	162	**12**	**0**
In	109	113	**7**	**0**
Tl	252	257	**43**	**41**
Si	151	208	**0**	**0**
Ge	191	205	**4**	**0**
Sn	144	147	**2**	**0**
Pb	168	175	**0**	**0**

[a]The energies are in the unit of meV/atom.

3.3. Electronic Structures of the Predicted Stable Metal Borohydride Compounds

We now focus on the basic electronic properties of the stable or metastable ternary metal borohydride compounds $X(BH_4)_3$ and $X(BH)_{12}$. Their electronic densities-of-states (DOS) for different elements in the compounds are shown in Figure 6 and 7, respectively.

We note that there is a great difference in the DOS values for different metal elements in each period. The compounds with the metal atoms from the group 2 and group 14 are semiconductors (or insulator) with wide band gaps of about 4 eV. By contrast, the compounds with metal elements from group 3 exhibit a very high DOS at the fermi level originating from the *d* state of the metals. There is a big gap ~5 eV in the DOS below the Fermi level. These compounds would be considered as heavily electron doped wide band gap semiconductions. It is interesting to note that the DOS of the compounds with group 13 metals (e.g., Al) displays an impurity-like peak right at the Fermi level. This peak is mainly contributed from the light B and H atoms. It would be interesting to investigate possible

superconducting behavior of these compounds.

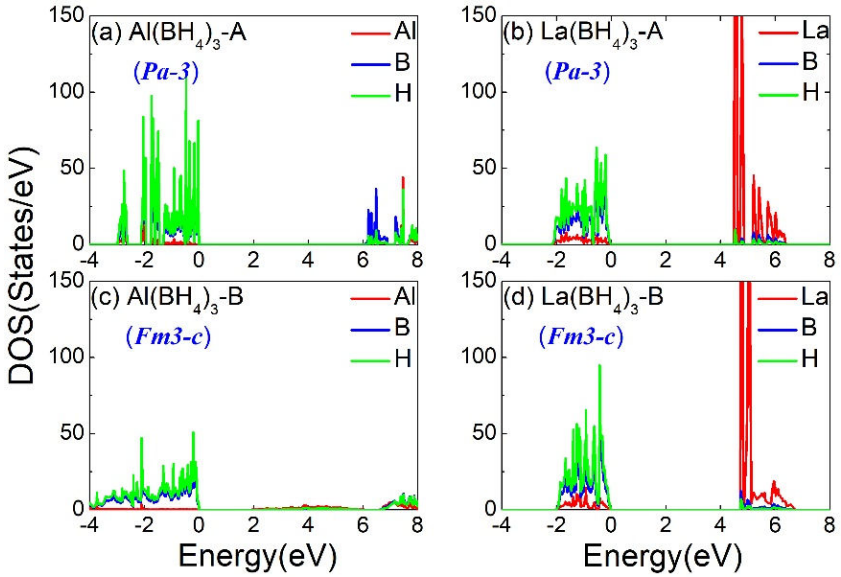

Figure 6. (Color online) Electronic density of states (DOS) for (a) $Al(BH_4)_3$-A (b) $La(BH_4)_3$-A (c) $Al(BH_4)_3$-B (d) $La(BH_4)_3$-B. Contributions of states from Al/La (red curve), B (blue curve) and H (green curve) are shown.

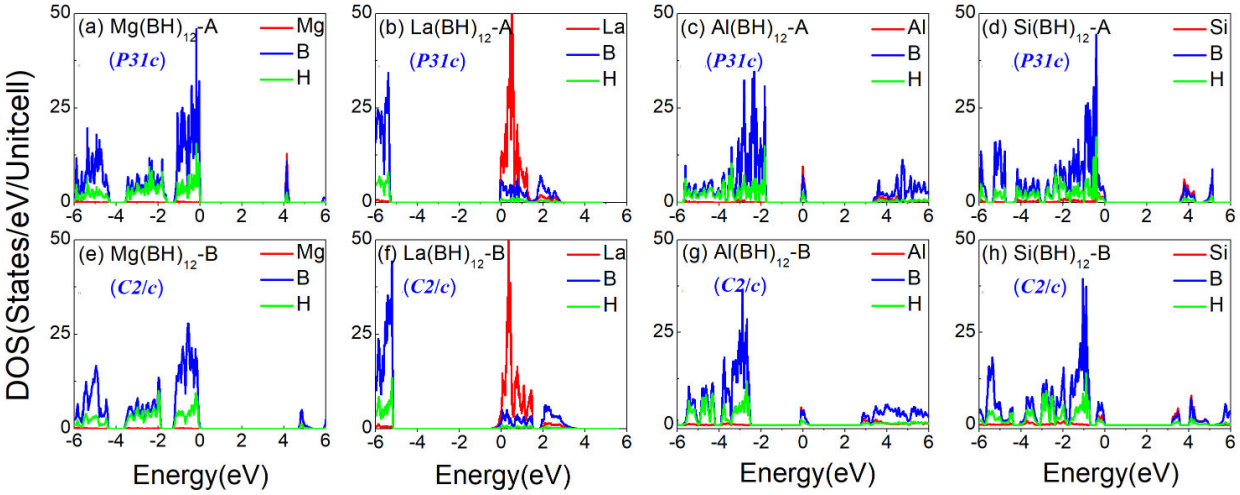

Figure 7. (Color online) Electronic density of states (DOS) for (a) $Mg(BH)_{12}$-A (b) $La(BH)_{12}$-A (c) $Al(BH)_{12}$-A (d) $Si(BH)_{12}$-A (e) $Mg(BH)_{12}$-B (f) $La(BH)_{12}$-B (g) $Al(BH)_{12}$-B (h) $Si(BH)_{12}$-B. Contributions of states from Mg/La/Al/Si (red curve), B (blue curve) and H (green curve) are shown.

4. Conclusion

By integrating deep ML with first-principles calculations, we successfully identify one known

$La(BH_4)_3$ (Pa-3 symmetry) compounds and uncover 30 new La-B-H ternary compounds with formation energies within 100 meV/atom above the convex hull, including a stable $La(BH)_{12}$ (P31c symmetry) phase. Moreover, substitutions of the La atom with Group 1, 2, 3, 13, and 14 elements reveal a series of low-energy ternary metal borohydrides. Using La-B-H as a prototype system, we demonstrate that iteratively trained ML models can comprehensively explore the composition-structure-property space of metal borohydrides and efficiently accelerate the discovery of novel materials.

Conflict of Interest

There are no conflicts of interest to declare.

Acknowledgments

This work was supported by the U.S. Department of Energy (DOE), Office of Science, Basic Energy Sciences, Materials Science and Engineering Division including a grant of computer time at the National Energy Research Scientific Computing Centre (NERSC) in Berkeley, CA. Ames Laboratory is operated for the U.S. DOE by Iowa State University under Contract No. DE-AC02-07CH11358. Rong Cheng and Xuyan Xue acknowledge the support by the Natural Science Foundation of Shandong Province (Grant No. ZR2023MB159).

References

[1] Ley, M. B.; Jepsen, L. H.; Lee, Y.-S.; Cho, Y. W.; von Colbe, J. M. B.; Dornheim, M.; Rokni, M.; Jensen, J. O.; Sloth, M.; Filinchuk, Y.; et al. Complex Hydrides for Hydrogen Storage – New Perspectives. *Materials Today* **2014**, *17*, 122-128.

[2] von Colbe, J. B.; Ares, J.-R.; Barale, J.; Baricco M.; Buckley, C.; Capurso, G.; Gallandat, N.; Grant, D. M.; Guzik, M. N.; Jacob. Isaac; et al. Application of Hydrides in Hydrogen Storage and Compression: Achievements, Outlook and Perspectives, *International Journal of Hydrogen Energy* **2019**, *44*, 7780-7808.

[3] Grinderslev, J. B.; Amdisen M. B.; Skov, L. N.; Møller, K. T.; Kristensen, L. G.; Polanski, M.; Heere M.; Jensen, T. R. New Perspectives of Functional Metal Borohydrides, *Journal of Alloys and Compounds* **2022**, *896*, 163014.

[4] Sheppard, D. A.; Paskevicius, M.; Humphries, T. D.; Felderhoff, M.; Capurso, G,; von Colbe, J. B.; Dornheim, M.; Klassen, T.; Ward, P. A.; Teprovich Jr., J. A.; et al. Metal Hydrides for Concentrating Solar Thermal Power Energy Storage, *Appl. Phys. A* **2016**, *122*, 395.

[5] Møller, K. T.; Sheppard, D.; Ravnsbæk, D. B.; Buckley, C. E.; Akiba, E.; Li, H.-W.; Jensen, T. R. Complex Metal Hydrides for Hydrogen, Thermal and Electrochemical Energy Storage. *Energies* **2017**, *10*,1645.

[6] Lu, Z.; Ciucci, F. Metal-Borohydrides as Electrolytes for Solid-State Li, Na, Mg and Ca Batteries: A First-Principles Study, *Chemistry of Materials* **2017**, *29*, 9308-9319.

[7] Aziam, H.; Larhrib, B.; Hakim, C.; Sabi, N.; Youcef, H. B.; Saadoune, I. Solid-State Electrolytes for beyond Lithium-Ion Batteries: A Review, *Renewable and Sustainable Energy Reviews* **2022**, *167*, 112694.

[8] Visseaux, M.; Bonnet, F. Borohydride Complexes of Rare Earths, and Their Applications in Various Organic Transformations, *Coordination Chemistry Reviews* **2011**, *255*, 374-420.

[9] Lyubov, D. M.; Tolpygin, A. O.; Trifonov, A. A. Rare-Earth Metal Complexes as Catalysts for Ring-Opening Polymerization of Cyclic Esters, *Coordination Chemistry Reviews* **2019**, *392*, 83-145.

[10] Richter, B.; Grinderslev, J. B.; Møller, K. T.; Paskevicius, M.; Jensen, T. R. From Metal Hydrides to Metal Borohydrides, *Inorg. Chem.* **2018**, *57*, 10768-10780.

[11] Wylezich, T.; Sontakke, A. D.; Castaing, V.; Suta, M.; Viana, B.; Meijerink, A.; Kunkel, N. One ion, many facets: Efficient, structurally and thermally sensitive luminescence of Eu2+ in binary and ternary strontium borohydride chlorides, *Chem. Mater.* **2019***, 31*, 8957-8968.

[12] Schouwink, P.; Didelot, E.; Lee, Y.-S.; Mazet, T.; Cerny, R. Structural and Magnetocaloric Properties of Novel Gadolinium Borohydrides, *Journal of Alloys and Compounds* **2016**, *664*, 378-384.

[13] Wegner, W.; J. van Leusen, J. van; Majewski, J.; Grochala, W.; Kögerler, P. Borohydride as Magnetic Superexchange Pathway in Late Lanthanide Borohydrides, *Eur. J. Inorg. Chem.* **2019**, *13*, 1776-1783.

[14] Gao, M.; Yan, X.-W.; Lu, Z.-Y.; Xiang, T. Phonon-Mediated High-Temperature Superconductivity in the Ternary Borohydride KB_2H_8 under Pressure near 12 GPa, *Phys. Rev. B: Condens. Matter Mater. Phys.* **2021**, *104*, L100504.

[15] Li, S.; Wang, H.; Sun, W.; Lu, C.; Peng, F. Superconductivity in Compressed Ternary Alkaline Boron Hydrides, *Phys. Rev. B: Condens. Matter Mater. Phys.* **2022**, *105*, 224107.

[16] Di Cataldo, S.; Boeri, L. Metal Borohydrides as Ambient-Pressure High-T_c Superconductors, *Phys. Rev. B: Condens. Matter Mater. Phys.* **2023**, *107*, L060501.

[17] Liu, X.; Zhang, L.; Wang, M.; Huang, X.; Liu, L.; Jia, Y. Realizing high-Tc ambient-pressure superconductivity in hole-doped hydride $Mg(BH_4)_2$, *Materials Today Physics* **2024**, *40*, 101299.
[18] Gao, M.; Guo, P.-J.; Yang, H.-C.; Yan, X.-W.; Ma, F.; Lu, Z.-Y.; Xiang, T.; Lin, H.-Q. Stabilizing a Hydrogen-Rich Superconductor at 1 GPa by Charge Transfer Modulated Virtual High-Pressure Effect, *Phys. Rev. B: Condens. Matter Mater. Phys*. **2023**, *107*, L180501.
[19] Łodziana, Z. Multivalent Metal Tetrahydroborides of Al, Sc, Y, Ti, and Zr, *Phys. Rev. B: Condens. Matter Mater. Phys.* **2010**, *81*, 144108.
[20] Frommen, C.; Sørby, M. H.; Heere, M.; Humphries, T. D.; Olsen, J. E,; Hauback, B. C. Rare Earth Borohydrides—Crystal Structures and Thermal Properties, *Energies* **2017**, *10*, 2115.
[21] Hwang, S.-J.; Bowman, R. C.; Reiter, J. W.; Rijssenbeek, J.; Soloveichik, G. L.; Zhao, J.-C.; Kabbour, H.; Ahn, C. C. NMR Confirmation for Formation of $[B_{12}H_{12}]^{2-}$ Complexes during Hydrogen Desorption from Metal Borohydrides, *J. Phys. Chem. C* **2008**, *112*, 3164-3169.
[22] Her, J.-H.; Yousufuddin, M.; Zhou, W.; Jalisatgi, S. S; Kulleck, J. G.; Zan, J. A.; Hwang, S.-J.; Bowman, R. C.; Udovic, T. J. Crystal Structure of $Li_2B_{12}H_{12}$: A Possible Intermediate Species in the Decomposition of $LiBH_4$, *Inorg. Chem*. **2008**, *47*, 9757-9759.
[23] Yan, Y.; Li, H.-W.; Maekawa, H.; Aoki, M.; Noritake, T.; Matsumoto, M.; Miwa, K.; Towata, S.; Orimo, S. Formation Process of $[B_{12}H_{12}]^{2-}$ from $[BH_4]^-$ during the Dehydrogenation Reaction of $Mg(BH_4)_2$, *Materials Transactions* **2011**, *52*, 1443-1446.
[24] Udovic, T. J.; Matsuo, M.; Unemoto, A.; Verdal, N.; Stavila, V.; Skripov, A. V.; Rush, J. J.; Takamura, H.; Orimo, S. Sodium Superionic Conduction in $Na_2B_{12}H_{12}$, *Chem. Commun*. **2014**, *50*, 3750-3752.
[25] Tang, W. S.; Unemoto, A.; Zhou, W.; Stavila, V.; Matsuo, M.; Wu, H.; Orimo, S.; Udovic, T. J. Unparalleled Lithium and Sodium Superionic Conduction in Solid Electrolytes with Large Monovalent Cage-like Anions, *Energy & Environmental Science* **2015**, *8*, 3637.
[26] Akrouchi, A.; Benzidi, H., Al-Shami, A.; El kenz, A.; Benyoussef, A.; El kharbachi, A.; Mounkachi, O. First-Principles Study of Closo-Dodecaborates $M_2B_{12}H_{12}$ (M = Li, Na, K) as Solid-State Electrolyte Materials, *Phys. Chem. Chem. Phys.* **2021**, *23*, 27014-27023.
[27] Suárez-Alcántara K.; García, J. R. T. Metal Borohydrides beyond Groups I and II: A Review, Materials **2021**, *14*, 2561.
[28] Deaven, D. M.; Ho, K. M. Molecular Geometry Optimization with a Genetic Algorithm, *Phys. Rev. Lett.* **1995**, *75*, 288-291.
[29] Zhao, X.; Nguyen, M. C.; Zhang, W. Y.; Wang, C. Z.; Kramer, M. J.; Sellmyer, D. J.; Li, X. Z.; Zhang, F.; Ke, L. Q.; Antropov, V. P.; et al. Exploring the Structural Complexity of Intermetallic Compounds by an Adaptive Genetic Algorithm, *Phys. Rev. Lett.* **2014**, *112*, 045502.
[30] Wang, Y.; Lv, J.; Zhu, L.; Ma, Y. CALYPSO: A Method for Crystal Structure Prediction, *Computer Physics Communications* **2012**, *183*, 2063-2070.
[31] Arapan, S.; Nieves, P.; Cuesta-López, S. A High-Throughput Exploration of Magnetic Materials by Using Structure Predicting Methods, *J. Appl. Phys.* **2018**, *123*, 083904.
[32] Shipley, A. M.; Hutcheon, M.; Needs, R. J.; Pickard, C. J. High-Throughput Discovery of High-Temperature Conventional Superconductors, *Phys. Rev. B: Condens. Matter Mater. Phys.* **2021***, 104,* 054501.
[33] Schleder, G. R.; Padilha, A. C. M.; Acosta, C. M.; Costa, M.; Fazzio, A. From DFT to Machine Learning: Recent Approaches to Materials Science – a Review, *Journal of Physics-Materials* **2019**, *2*, 032001.

[34] Xie T.; Grossman, J. C. Crystal Graph Convolutional Neural Networks for an Accurate and Interpretable Prediction of Material Properties, *Phys. Rev. Lett.* **2018**, *120*, 145301.
[35] Wang, R.; Xia, W.; Slade, T. J.; Fan, X.; Dong, H.; Ho, K.-M.; Canfield, P. C.; Wang, C.-Z. Machine Learning Guided Discovery of Ternary Compounds Involving La and Immiscible Co and Pb Elements, *NPJ Computational Materials* **2022**, *8*, 258.
[36] Sun, H.; Zhang, C.; Xia, W.; Tang, L.; Wang, R.; Akopov, G.; Hewage, N. W.; Ho, K.-M.; Kovnir, K.; Wang, C. Z. Machine Learning-Guided Discovery of Ternary Compounds Containing La, P, and Group 14 Elements, *Inorg. Chem.* **2022,** *61*, 16699-16706.
[37] Xia, W.; Sakurai, M.; Balasubramanian, B.; Liao, T.; Wang, R.; Zhang, C.; Sun, H.; Ho, K.-M.; Chelikowsky, J. R.; Sellmyer, D. J.; et al. Accelerating the Discovery of Novel Magnetic Materials Using Machine Learning–Guided Adaptive Feedback, *Proceedings of the National Academy of Sciences* **2022**, *119*, e2204485119.
[38] Zhang, C.; Tang, H.; Pan, C.; Jiang, H.; Sun, H.-J.; Ho, K.-M.; Wang, C.-Z. Machine learning guided discovery of superconducting calcium borocarbides, *Phys. Rev. B: Condens. Matter Mater. Phys.* **2023**, *108*, 024512.
[39] Kresse, G.; Joubert, D. From Ultrasoft Pseudopotentials to the Projector Augmented-Wave Method, *Phys. Rev. B: Condens. Matter Mater. Phys.* **1999**, *59*, 1758-1775.
[40] Kresse, G.; Furthmüller, J. Efficient Iterative Schemes for Ab Initio Total-Energy Calculations Using a Plane-Wave Basis Set, *Phys. Rev. B: Condens. Matter Mater. Phys.* **1996**, *54*, 11169-11186.
[41] Perdew, J. P.; Burke, K.; Ernzerhof, M. Generalized Gradient Approximation Made Simple, *Phys. Rev. Lett.* **1996**, *77*, 3865-3868.
[42] Monkhorst, H. J.; Pack, J. D. Special Points for Brillouin-zone Integrations, *Phys. Rev. B: Condens. Matter Mater. Phys.* **1976***, 13,* 5188-5192.
[43] Her, J.-H.; Wu, H.; Verdal, N.; Zhou W.; Stavila, V.; Udovic, T. J. Structures of the Strontium and Barium Dodecahydro-Closo-Dodecaborates, *Journal of Alloys and Compounds* **2012**, *514*, 71-75.
[44] Stavila, V.; Her, J.-H.; Zhou, W.; Hwang, S.-J.; Kim, C.; Ottley, L. A. O.; Udovic, T. J. Probing the structure, stability and hydrogen storage properties of calcium dodecahydro-closo-dodecaborate, *Journal Solid State Chemistry* **2010**, *183,*1133-1140.
[45] Her, J.-H.; Zhou, W.; Stavila, V.; Brown, C. M.; and Udovic, T. J. Role of Cation Size on the Structural Behavior of the Alkali-Metal Dodecahydro-Closo-Dodecaborates, *J. Phys. Chem. C* **2009**, *113*, 11187-11189.

TOC Graphic

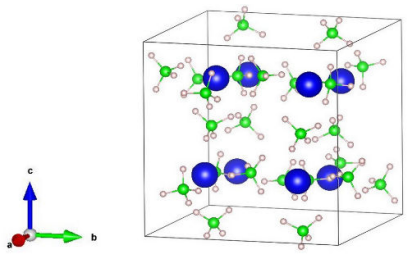

$La(BH_4)_3$-A Pa-3

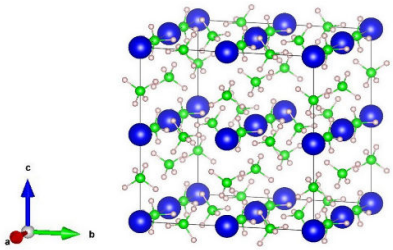

$La(BH_4)_3$-B Fm3-c

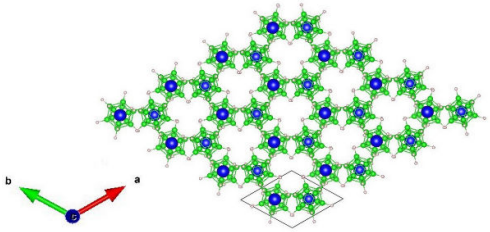

$La(BH)_{12}$-A P31c

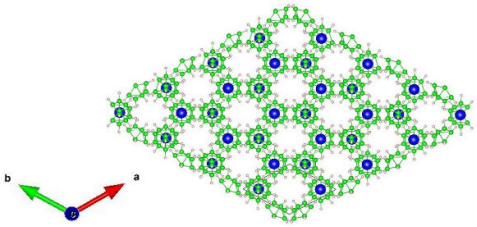

$La(BH)_{12}$-B C2/c